Experiments in Fluids 25 (1998) 316–319

A particle image velocimetry system for microfluidics

J. G. Santiago, S. T. Wereley, C. D. Meinhart, D. J. Beebe, R. J. Adrian

Abstract A micron-resolution particle image velocimetry (micro-PIV) system has been developed to measure instantaneous and ensemble-averaged flow fields in micron-scale fluidic devices. The system utilizes an epifluorescent microscope, 100–300 nm diameter seed particles, and an intensified CCD camera to record high-resolution particle-image fields. Velocity vector fields can be measured with spatial resolutions down to $6.9 \times 6.9 \times 1.5$ μm. The vector fields are analyzed using a double-frame cross-correlation algorithm. In this technique, the spatial resolution and the accuracy of the velocity measurements is limited by the diffraction limit of the recording optics, noise in the particle image field, and the interaction of the fluid with the finite-sized seed particles. The stochastic influence of Brownian motion plays a significant role in the accuracy of instantaneous velocity measurements. The micro-PIV technique is applied to measure velocities in a Hele–Shaw flow around a 30 μm (major diameter) elliptical cylinder, with a bulk velocity of approximately 50 μm s^{-1}.

1 Introduction

Over the past ten years, significant progress has been made in the development of microfluidic devices based on microelectromechanical system (MEMS) technologies, such as bioanalysis systems, flow sensors, micro-valves, and micropropulsion schemes (Gravesen et al. 1993; Brody et al. 1996). The scientific community has witnessed an explosive surge of miniaturization schemes and designs. However, relatively few studies have specifically addressed the physics related to scaling down engineering systems. This trend is particularly true of microfluidic systems, whose designs are strongly influenced by the effects of high dissipation rates, decreased volume-to-surface area ratio (e.g., surface tension phenomena), and electrohydrodynamic phenomena.

Since the flow passages of MEMS microfluidic devices have length scales of order 1–100 μm, traditional flow diagnostic tools cannot be used. Most measurements in microfluidic devices have been limited to bulk properties of the flow, such as wall pressure, bulk velocity, and specific impulse (in the case of micronozzles). An exception can be found in the measurements of Brody et al. (1996), who used an intensified CCD camera to image particle streaks in an 11×72 μm (cross section) silicon channel. In practice, image streaks are difficult to analyze numerically. Velocity measurements determined from particle streaks are less reliable and are about ten times less accurate than pulsed velocimetry measurements (Adrian 1991).

The microflow measurement technique demonstrated by Lanzilloto et al. (1997) uses X-ray micro-imaging techniques to measure velocity fields in 500–1000 μm diameter micro-tubes by recording the motion of 1–20 μm emulsion droplets in a liquid flow. Velocity fields are estimated by tracking the trajectories of the emulsion droplets over time. Lanzillotto et al. (1996) reported mean velocity fields in an 840 μm diameter tube, with velocity-vector spacings of about 40 μm and axial bulk velocities of 7–14 μm s^{-1}. The primary advantage of this technique is the ability to obtain internal fluid velocities without optical access. Since the emulsion droplets are deformable, polydispersed, and relatively large, the fidelity with which the droplets follow the flow field and the accuracy with which one can determine velocity vectors are of concern. Another group (Chen et al., 1997) has used Optical Doppler Tomographic imaging to obtain velocity measurements using Michelson interferometry. These investigators used 1.7 μm diameter seed particles with a $5 \times 5 \times 15$ μm measurement volume. Unfortunately, this technique is limited to single point measurements.

2 Experimental technique

2.1 Flow-tracing particles

In micro-PIV, seed particle size must be small enough to faithfully follow the flow without disrupting the flow field,

Received: *26 November 1997*/*Accepted*: *26 February 1998*

J. G. Santiago, D. J. Beebe
Department of Electrical and Computer Engineering, Beckman Institute for Advanced Science and Technology, 4265 Beckman Institute, University of Illinois, Urbana, IL 61801, USA

S. T. Wereley, C. D. Meinhart
Department of Mechanical and Environmental Engineering, University of California, Santa Barbara, CA 93106, USA

R. J. Adrian
Department of Theoretical and Applied Mechanics, University of Illinois, Urbana, IL 61801, USA

Correspondence to: J. G. Santiago

This work is supported by University of Illinois Beckman Institute for Advanced Science and Technology, a Ford Foundation Post-Doctoral Fellowship, and by AFOSR/DARPA grant number F49620-97-1-0515 under the direction of Dr. Mark Glauser.

clogging the device, and producing unnecessarily large images. At the same time, particles must be large enough to be adequately imaged and to dampen the effects of Brownian motion. For the current experiments, we chose 300 nm diameter polystyrene particles manufactured by Bangs Laboratory with a specific gravity of $\rho_p = 1.055$. These particles are tagged with a fluorescent dye that absorbs at a wavelength of $\lambda_{abs} = 469$ nm (blue) and emits at a peak of $\lambda_{emit} = 509$ nm (green).

Brownian motion is an important consideration when using sub-micron particles to trace velocity fields of order 10 μm s^{-1}. Given time intervals, Δt, much larger than the particle relaxation time τ_p (which is of order 10^{-9} s in our case), the mean square distance of diffusion is

$$\langle s^2 \rangle = 2D\,\Delta t \tag{1}$$

where the diffusion coefficient, first derived by Einstein (1905), is given as

$$D = \frac{\kappa T}{3\pi\mu d_p} \tag{2}$$

Here, d_p is the particle diameter, κ is Boltzman's constant, T is the absolute temperature of the fluid, and μ is the dynamic viscosity of the fluid. In regions where velocity gradients are small, the effect of Brownian diffusion can be modeled as a white-noise process that increases the uncertainty in which the displacement of a particle can be measured. A particle following faithfully a steady flow with velocity u over a time interval Δt has a displacement

$$\Delta x = u\,\Delta t. \tag{3}$$

Therefore, the relative error due to Brownian motion can be estimated by

$$\varepsilon_B = \frac{\langle s^2 \rangle^{1/2}}{\Delta x} = \frac{1}{u}\sqrt{\frac{2D}{\Delta t}} \tag{4}$$

This error establishes a lower limit on the desired measurement time interval, Δt. In regions where velocity gradients are large, the errors associated with Brownian motion become much more complicated. This type of error places an upper limit on Δt. This effect will be discussed in a future paper.

In the current experiments, the characteristic velocity is $u \sim 50$ μm s^{-1} and $\Delta t = 68.5$ ms; this yields a relative error due to Brownian motion of approximately 9%. Since this error is a result of diffusion, it is unbiased and can be substantially reduced by averaging over several particle images in a single interrogation spot and by ensemble averaging over several realizations. Assuming each particle contributes equally to the average velocity vector, and that each measurement is statistically independent, the diffusive uncertainty is then proportional to $\varepsilon_B/\sqrt{N}$, where N is the total number of particles in the average. In the current measurements, there were approximately five particle images per interrogation spot, and eight instantaneous realizations were used to ensemble-average the vector field. This yields $N = 40$ independent samples or approximately 1.4% uncertainty in the ensemble-averaged velocity.

2.2 Imaging and Recording

In microscopy, object distances are on the order of the collection aperture, and the typical measure of collection efficiency is the numerical aperature, *NA*, defined as

$$NA = n \sin\phi \tag{5}$$

where n is the refractive index of the immersing medium adjacent to the objective lens and ϕ is the angular radius of the collection cone. The square of NA determines the light-gathering power of the recording system. In contrast, the collection lenses in most traditional PIV systems are designed to image objects at distances much larger than the aperture of the lens, and the common measure of the collection efficiency is *f*-number (equal to the focal length-to-aperture ratio). For the special case where the medium surrounding the lens is air ($n = 1$) and the object distance is large compared to the aperture of the lens, *NA* can be approximately related to *f*-number by

$$NA = (2\,f\text{-number})^{-1} \quad \text{(Born and Wolf 1991)} \tag{6}$$

Figure 1 shows a schematic of the imaging system used in the present experiments. The microfluidic system is loaded onto an Olympus epifluorescent microscope equipped with a mercury lamp and color filters for microscopic fluorescence imaging. The microscope is fitted with a 100 × magnification, oil-immersion objective with a numerical aperture (NA) of 1.4 (note that, for this high-resolution lens, Eq. (6) does not apply). Particle images were recorded using a Princeton Instruments Pentamax 512 EFT intensified CCD camera with a 512 × 512 pixel array and 12 bit resolution. The microchannel plate in the CCD camera (which is used to gate the images) intensifies the weak fluorescence signal by a factor of 10^3–10^4 at the expense of introducing white noise into the image. In the current experiment, the CCD array was exposed for $\delta t = 2$ ms, and the time delay between successive images was $\Delta t = 68.5$ ms.

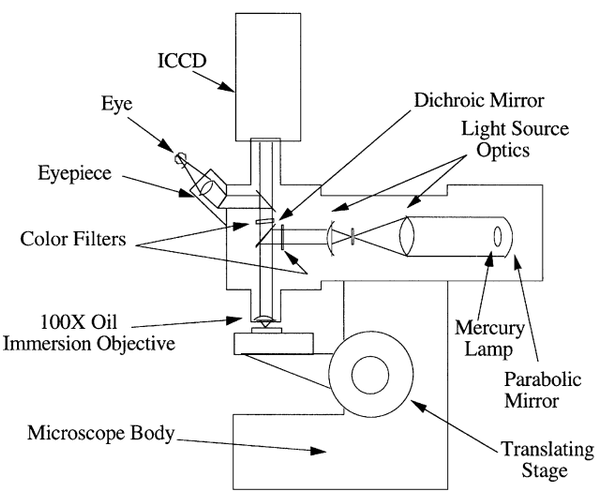

Fig. 1. Schematic of the micro-PIV recording system using: (1) an epifluorescent microscope, (2) a high numerical aperture lens, (3) a continuous-illumination mercury arc lamp, and (4) an intensified/cooled CCD camera

In most PIV systems, the measurement domain in the out-of-plane direction is defined by the thickness of an illuminating light sheet. Because such an arrangement is often impractical in microfluidic systems, the present work defines the measurement domain by the relatively small depth-of-field of the $NA = 1.4$ lens. Note that the microscope is fitted with a micron-resolution positioning system that can be used to measure out-of-plane dimensions and to translate the measurement volume. Given a criteria of less than 25% increase in particle image diameter, the depth-of-field for the system was measured to be approximately 1.5 μm. Particles outside of this depth-of-field are at least 25% larger than in-focus particles and have substantially lower image intensities. We filter most of this out-of-field noise by thresholding the image intensity field so that particles outside of the depth-of-field do not contribute significantly to the cross-correlations of image intensity.

The recorded image of a seed particle is a convolution of the geometric particle image, Md_p, with the point-spread function, d_s, of the recording optics. The characteristics diameter of the point-spread function is

$$d_s = 1.22(1+M)\lambda NA^{-1} \tag{7}$$

where M is the magnification and λ is the wavelength of light (Born and Wolf 1991). Approximating d_s and Md_p as Gaussians, the image diameter, d_e, can be expressed as

$$d_e = [M^2 d_p^2 + d_s^2]^{1/2}. \tag{8}$$

For spherical 300 nm particles emitting in the green and imaged with an $NA = 1.4$ and $M = 100$ objective lens, the image diameter is 54 μm. The image diameter projected back into the flow field is approximately 540 nm.

2.3 Refining the resolution of a micro-PIV system

If the diameter of a particle image is resolved over 3–4 pixels, then the uncertainty in determining particle displacement can be found to within one tenth of the particle-image diameter (Prasad et al., 1992). In the present experiment, the uncertainty in determining particle image displacement is estimated to be approximately 54 nm. In other words, since the *shape* of the particles is known *a priori*, the relative position of the seed particles can be determined with a resolution 10 times greater than the diffraction-limited resolution of the microscope.

The resolution of micro-PIV measurements can be increased further by employing super-resolution PIV (Keane et al. 1995). In this technique, correlation analysis is first used to determine the average velocity of groups of particles in single interrogation regions. This information is then fed into a particle tracking velocimetry (PTV) algorithm to determine the displacement of individual particles. In principle, super-resolution PIV can be used to extend the spatial resolution of velocity measurements down to approximately $1.2 \times 1.2 \times 1.5$ μm.

2.4 Hele–Shaw cell

A simple liquid Hele–Shaw flow field was used to demonstrate the micro-PIV technique. The Hele–Shaw flow was established by placing a drop of deionized, surfactanated water seeded with 300 nm diameter polystyrene particles between the frosted region of a microscope slide and a clear 170 μm thick coverslip. The liquid layer between the microscope slide and the coverslip was measured to be approximately 5 μm. Evaporation and wicking of the water on exposed regions of the frosted glass established a relatively steady flow field with velocities on the order of 10 μm s^{-1}. Higher flow velocities were achieved by placing a small drop of water at the coverslip's edge. The surface elements of the frosted slide create 10–100 μm wide obstacles in the flow cell.

Hele–Shaw flow is a steady, low Reynolds number flow that obeys the Stokes flow equations. The Reynolds number (based on the 5 μm separation distance and the approaching bulk flow velocity) for the presented flow field was 3×10^{-4}. An interesting feature of this flow field is that planes parallel to the top and bottom boundaries have streamlines which coincide with streamlines of hypothetical two-dimensional potential flow fields with similar geometries (Batchelor 1967). However, because of the non-slip condition, the potential flow approximation of horizontal planes breaks down at distances on the order of the separation distance (5 μm in our case) from the obstacle boundaries.

3 Results

Images were interrogated using a conventional interrogation algorithm developed at the University of California at Santa-Barbara and a commercially-available algorithm from TSI Inc. Results from both of these algorithms agreed. Figure 2a shows an instantaneous vector field measurement of a Hele–Shaw flow around an obstruction that can be approximately described as an elliptical cylinder with major and minor axes of 20 and 25 μm, respectively. Most of the noise in this velocity field measurement is due to the influences of Brownian motion and image noise. Ensemble averaging several measurements substantially reduces this unbiased noise and yields the velocity data shown in Fig. 2b. This ensemble consists of eight instantaneous measurements and was calculated on a point-by-point basis. Regions in the instantaneous fields where valid vectors could not be obtained were excluded from the averaging calculation. In all of the flow measurements, the approaching mean velocity is 35 μm s^{-1} (at the midplane) from the lower left to the upper right. The interrogation spots were 32×32 pixels with a cross-correlation window offset of six pixels in both the horizontal and vertical directions. Each interrogation spot was overlapped by 50%, producing approximately 900 vectors over a 120 μm × 120 μm field. The spatial resolution is defined by the $6.9 \times 6.9 \times 1.5$ μm interrogation volume (which corresponds to a 3.45 μm vector-to-vector distance for 50% overlap).

The velocity vector field measurements capture many of the features of the 3×10^{-4} Reynolds number Hele–Shaw flow. First, the flow field exhibits the inherent in-plane, symmetry of flow motion characteristics of low Reynolds number flows. Second, the measurements show the limitation of the potential flow analogy very near the boundary of the obstacle: Note the in-plane velocity gradients near the obstacle boundary that result from the no-slip condition. Third, the measurements

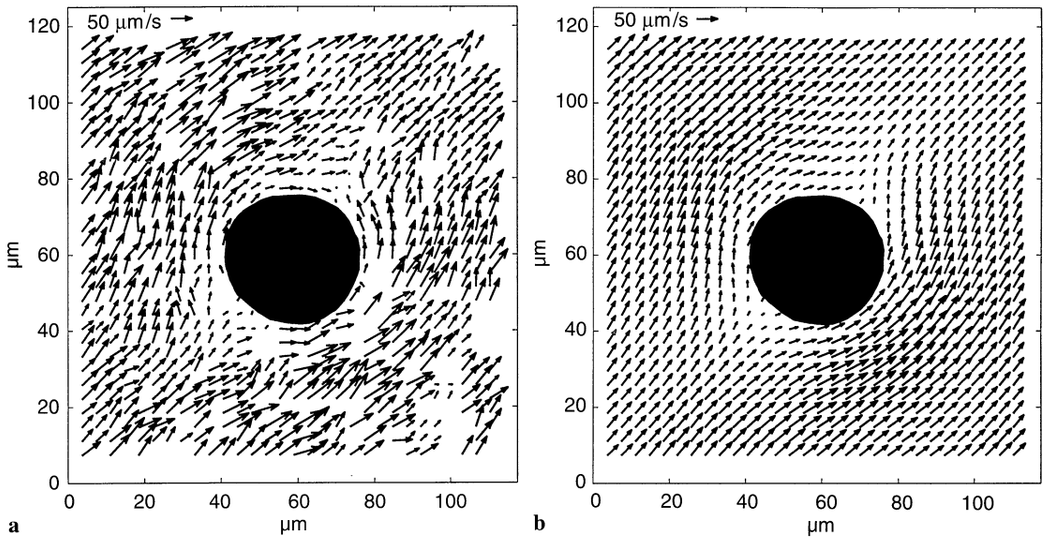

Fig. 2a,b. Vector fields of a surface-tension driven Hele–Shaw flow around a 30 μm wide obstacle. Each field contains approximately 900 velocity vectors covering a 120 μm × 120 μm field of view. Each velocity vector was measured with a 6.9 μm × 6.9 μm × 1.5 μm measurement volume. **a** Instantaneous vector field measurement. **b** Eight-image ensemble-averaged PIV velocity vector field

clearly resolve the locations of the two stagnation points on either side of the cylindrical obstruction.

4 Conclusions

A micro-PIV technique has been developed and demonstrated that is capable of providing measurements of velocity fields with 3.45 μm vector-to-vector distances using a $6.9 \times 6.9 \times 1.5$ μm interrogation volume. In principle, this technique can be refined to provide ensemble-averaged velocity fields with spatial resolutions approaching one micron. The technique uses epifluorescent microscopy and an intensified CCD camera to image 100–300 nm diameter, fluorescently tagged polystyrene particles. Measurements are presented that resolve many features of a 3×10^{-4} Reynolds number Hele–Shaw flow field around a roughly cylindrical obstruction with a 30 μm axis. These features include the locations of stagnation points and high in-plane velocity gradients near the obstruction's boundary. Using this micro-PIV technique, the spatial resolution and the accuracy of the fluid velocity measurements is limited by the diffraction limit of the recording optics, noise in the particle-image field, the interaction of the fluid with the finite-sized seed particles, and Brownian motion.

References

Adrian RJ (1991) Particle-imaging techniques for experimental fluid mechanics. Ann Rev Fluid Mech 23: 261–304

Batchelor GK (1987) An introduction to fluid dynamics. Cambridge University Press, Cambridge

Born M; Wolf E (1991) Principles of Optics. Pergamon Press, Oxford

Brody JP; Yager P; Goldstein RE; Austin RH (1996) Biotechnology at Low Reynolds numbers. Biophys J 71: 3430–3441

Chen Z; Milner TE; Dave D; Nelson JS (1997) Optical Doppler tomographic imaging of fluid flow velocity in highly scattering media. Opt Lett 22: 64–66

Einstein A (1905) On the movement of small particles suspended in a stationary liquid demanded by the molecular-kinetic theory of heat. In: Theory of the Brownian Movement, Dover Publications, Inc, New York, pp 1–18

Gravesen P; Branebjerg J; Jensen OS (1993) Microfluidics – a review. J Micromech Microeng 3

Keane RD; Adrian RJ; Zhang Y (1995) Super-resolution particle imaging velocimetry. Meas. Sci. Tech. 6: 754–768

Lanzillotto A-M; Leu T-S; Amabile M; Samtaney R; Wildes R (1997) A study of structure and motion in fluidic microsystems. AIAA Paper 97-1790, 28th Fluid Dynamics Conf, Snowmass Village, CO, June 29–July 2

Prasad AK; Adrian RJ; Landreth CC; Offutt PW (1992) Effect of resolution on the speed and accuracy of particle image velocimetry interrogation. Exp Fluids 13: 105–116